The Astronomical Journal, 132:2743–2754, 2006 December

CHARACTERIZING THREE CANDIDATE MAGNETIC CATACLYSMIC VARIABLES FROM SDSS: *XMM-NEWTON* AND OPTICAL FOLLOW-UP OBSERVATIONS[1]

Lee Homer,[2] Paula Szkody,[2] Arne Henden,[3,4,5] Bing Chen,[6,7] Gary D. Schmidt,[8]
Oliver J. Fraser,[2] and Andrew A. West[2]

Received 2006 May 31; accepted 2006 August 29

ABSTRACT

In the latest in our series of papers on *XMM-Newton* and ground-based optical follow-up of new candidate magnetic cataclysmic variables (mCVs) found in the Sloan Digital Sky Survey, we report classifications of three systems: SDSS J144659.95+025330.3, SDSS J205017.84−053626.8, and SDSS J210131.26+105251.5. Both the X-ray and optical fluxes of SDSS J1446+02 are modulated on a period of 48.7 ± 0.5 minutes, with the X-ray modulation showing the characteristic energy dependence of photoelectric absorption seen in many intermediate polars (IP). A longer period modulation and radial velocity variation is also seen at around 4 hr, although neither data set is long enough to constrain this longer, likely orbital, period well. SDSS J2050−05 appears to be an example of the most highly magnetized class of mCV, a diskless, stream-fed polar. Its 1.57 hr orbital period is well constrained via optical eclipse timings; in the X-ray it shows both eclipses and an underlying strong, smooth modulation. In this case broadly phase-resolved spectral fits indicate that this change in flux is the result of a varying normalization of the dominant component (a 41 keV MEKAL plasma), plus the addition of a partial covering absorber during the lower flux interval. SDSS J2101+10 is a more perplexing system to categorize: its X-ray and optical fluxes exhibit no large periodic modulations; there are only barely detectable changes in the velocity structure of its optical emission lines; the X-ray spectra require only absorption by the interstellar medium; and the temperatures of the MEKAL fits are low, with maximum temperature components of either 10 or 25 keV. We conclude that SDSS J2101+10 cannot be an IP, nor likely a polar, but is rather most likely a disk accretor—a low-inclination SW Sex star.

Key words: novae, cataclysmic variables — stars: individual (SDSS J144659.95+025330.3, SDSS J205017.84−053626.8, SDSS J210131.26+105251.5) — stars: magnetic fields — X-rays: stars

Online material: color figures

1. INTRODUCTION

The Sloan Digital Sky Survey (SDSS; York et al. 2000) has provided a wealth of new cataclysmic variables (CVs), the close binary systems with active accretion from a late main-sequence star to a white dwarf (reviewed in Warner 1995). Due to its sensitivity down to ∼21 mag, SDSS is especially suited to the discovery of faint CVs with low accretion rates and short orbital periods. Included in the discoveries are dozens of systems with a noticeable emission line of He II, which is often a signature of a white dwarf with a high magnetic field. The highest field systems (polars) have no accretion disk, and the white dwarf spin is synchronized to the orbit. The intermediate polars (IPs) usually have some outer disk, with magnetic curtains channeling the inner disk material to the magnetic poles of the white dwarf, which is spinning faster than the orbital timescale. Polars can be identified by circular polarization, cyclotron harmonics, and/or Zeeman splitting (review in Wickramasinghe & Ferrario 2000), while IPs are found through the detection of their spin and orbital periods. In addition, there is a class of high accretion rate disk systems with possible low magnetic field white dwarfs (Rodríguez-Gil et al. 2001) termed SW Sex stars that can also show strong He II lines in their optical spectra.

For the last few years we have used *XMM-Newton* to identify the nature of CVs with He II and to explore the nature of X-ray heating in these systems. Polars generally exhibit hard X-rays from the accretion shock and soft X-rays from the white dwarf surface heated by the hard X-rays. The ratio of soft to hard X-rays shows a dramatic change with magnetic field strength and accretion rate. The IPs are generally hard X-ray emitters with large absorption effects from the accretion curtains. Usually the spin period is much more pronounced in the X-ray than the optical. The SW Sex stars usually show no X-ray variation and are hard X-ray emitters with low absorption.

The three sources in this study are all about 18 mag in the SDSS *g* filter and were all identified as potential magnetic CVs in Szkody et al. (2003a). SDSS J144659.95+025330.3 (hereafter SDSS J1446+02) showed no polarization, and limited time-resolved spectra could not determine the orbital period. SDSS J205017.85−053626.8 (SDSS J2050−05) has the strongest He II line of the three objects, with a peak flux comparable to Hβ, and showed evidence of high and low states of mass transfer. A short span of time-resolved spectroscopy showed an orbital period near 2 hr. Follow-up high-speed photometry by Woudt et al. (2004) revealed brief (260 s), deep (1.5 mag) eclipses and determined a precise period of 1.57 hr. The third system, SDSS J210131.26+105251.5 (SDSS J2101+10), has very strong Balmer lines but did not show any velocity variation during 1.3 hr of time-resolved spectroscopy.

[1] Based on observations obtained with the Sloan Digital Sky Survey and with the Apache Point Observatory 3.5 m telescope, which are owned and operated by the Astrophysical Research Consortium.

[2] Department of Astronomy, University of Washington, Seattle, WA, USA.
[3] Universities Space Research Association.
[4] US Naval Observatory, Flagstaff Station, Flagstaff, AZ, USA.
[5] American Association of Variable Star Observers, Cambridge, MA, USA.
[6] *XMM-Newton* Science Operations Centre, ESA/Vilspa, Madrid, Spain.
[7] VEGA Information-Technologien GmbH, Darmstadt, Germany.
[8] Steward Observatory, The University of Arizona, Tucson, AZ, USA.

Report Documentation Page

Form Approved
OMB No. 0704-0188

1. REPORT DATE	2. REPORT TYPE	3. DATES COVERED
DEC 2006	**N/A**	**-**

4. TITLE AND SUBTITLE	5a. CONTRACT NUMBER
Characterizing Three Candidate Magnetic Cataclysmic Variables From SDSS: XMM-Newton and Optical Follow-Up Observations	5b. GRANT NUMBER
	5c. PROGRAM ELEMENT NUMBER
6. AUTHOR(S)	5d. PROJECT NUMBER
	5e. TASK NUMBER
	5f. WORK UNIT NUMBER
7. PERFORMING ORGANIZATION NAME(S) AND ADDRESS(ES) **U.S. Naval Observatory Library 3450 Massachusetts Avenue, N.W. Washington, DC 20392-5420**	8. PERFORMING ORGANIZATION REPORT NUMBER
9. SPONSORING/MONITORING AGENCY NAME(S) AND ADDRESS(ES)	10. SPONSOR/MONITOR'S ACRONYM(S)
	11. SPONSOR/MONITOR'S REPORT NUMBER(S)

12. DISTRIBUTION/AVAILABILITY STATEMENT
Approved for public release, distribution unlimited

13. SUPPLEMENTARY NOTES

14. ABSTRACT

15. SUBJECT TERMS

16. SECURITY CLASSIFICATION OF:			17. LIMITATION OF ABSTRACT	18. NUMBER OF PAGES	19a. NAME OF RESPONSIBLE PERSON
a. REPORT	b. ABSTRACT	c. THIS PAGE			
unclassified	**unclassified**	**unclassified**	**SAR**	**12**	

TABLE 1
OBSERVATION SUMMARY

UT Date	Observatory	UT Time	Characteristics[a]	Comments
		SDSS J1446+02		
2002 May 11	SO Bok (2.3 m)	...	$v = +0.38\%$	3 ks exposure, spectropolarimetry
2003 Apr 27	APO	05:43–09:47	...	23×600 s spectra
2003 May 7	NOFS	06:39–11:34	$\sim V = 17.9$	Open filter photometry
2004 Jan 30	*XMM-Newton* EPIC-pn	04:17–05:32	0.2 counts s^{-1}	Only 3.0 ks live time[b,c]
	XMM-Newton EPIC-MOS1/2	03:55–05:18	0.1 counts s^{-1}	Only 4.5 ks live time[c]
	XMM-Newton OM	04:03–08:10	$B = 18.3$	13.9 ks duration
	NOFS	09:13–13:18	$\sim V = 18.2$	Open filter photometry
2005 Jan 12	*XMM-Newton* EPIC-pn	06:22–08:09	0.20 counts s^{-1}	5.6 ks live time
	XMM-Newton EPIC-MOS1/2	06:00–08:14	0.10 counts s^{-1}	7.7 ks live time
	XMM-Newton OM	06:08–08:16	$B = 18.2$	5.6 ks duration
		SDSS J2050−05		
2003 May 29	MMT	...	$v = +1.06\%$	1.2 ks exposure, spectropolarimetry
2003 May 30	MMT	...	$v = -0.23\%$	2.4 ks exposure, spectropolarimetry
2004 May 14	SO Bok (2.3 m)	...	$v = -0.31\%$	1.2 ks exposure, spectropolarimetry
2004 Oct 18	*XMM-Newton* EPIC-pn	10:13–13:17	0.67 counts s^{-1}	8.7 ks live time[b]
	XMM-Newton EPIC-MOS1/2	09:50–13:22	0.21 counts s^{-1}	12 ks live time
	XMM-Newton OM	06:08–08:16	$B = 18.4$	8.4 ks duration
2004 Oct 21	NOFS	01:33–04:34	$\sim V = 18.0$	Open filter photometry
		SDSS J2101+10		
2003 May 29	SO Bok (2.3 m)	...	$v = +0.03\%$	1.6 ks exposure, spectropolarimetry
2003 Sep 22	SO Bok (2.3 m)	...	$v = +0.10\%$	1.6 ks exposure, *R*-band imaging polarimetry
2004 May 14	APO	10:47–11:04	...	1 ks spectrum
2004 May 19	NOFS	08:01–11:35	$\sim V = 18.9$	Open filter photometry
2004 May 19	*XMM-Newton* EPIC-pn	16:57–18:13	0.64 counts s^{-1}	4.1 ks live time[b]
	XMM-Newton EPIC-MOS1/2	16:35–18:18	0.23 counts s^{-1}	6.1 ks live time
	XMM-Newton OM	16:43–18:20	$B = 19.0$	5.5 ks duration

[a] The open-filter photometry from NOFS has an estimated equivalent *V* zero point, while for spectra the flux density at ~5500 Å is used. The *XMM-Newton* count rates are average values for each observation for a single detector.
[b] The live time of the X-ray CCD detectors refers to the sum of the GTIs, less any dead time. It is typically much less than the difference of observation start and stop times.
[c] These X-ray exposures were curtailed by severe particle background flaring.

The *XMM-Newton* data obtained on these three sources, combined with additional photometry, spectroscopy, and spectropolarimetry, have allowed us to determine that SDSS J1446+02 is an IP and SDSS J2050−05 is a likely polar, while SDSS J2101+10 escapes an easy classification but appears most likely to be an SW Sex star. Our observations and results are described below.

2. OBSERVATIONS

2.1. *X-Ray*

Table 1 summarizes our X-ray and optical observations. SDSS J1446+02 was observed twice by *XMM-Newton*, as the 2004 January 30 observation was badly affected by high charged-particle background throughout, and the X-ray exposures were curtailed after only a few kiloseconds. Since the X-ray instrumentation (comprising three X-ray telescopes, backed by the two MOS and one pn EPIC CCD cameras; Turner et al. 2001) was set as the prime instrument, an automatic reobservation was triggered. However, the 2004 optical data from *XMM-Newton*'s optical monitor (OM; Strüder et al. 2001) were good throughout the scheduled ~13 ks observation. In the second observation, on 2005 January 12, good data were obtained from all three EPIC spectroimagers, but this time the OM only succeeded for two out of an expected four exposures. We note that for both observations no useful data were available from the two Reflection Grating Spectrographs (RGSs; den Herder et al. 2001) arrayed in the optical path of the MOS detectors, as the source is too faint to furnish adequate signal in the dispersed spectra. The initial visits made to SDSS J2050−05 and SDSS J2101+10 were highly successful, with only a little background flaring in the last 3 ks of the 12 ks observation of SDSS J2050−05 and none affecting that of SDSS J2101+10. Useful data were therefore obtained from EPIC imaging and the OM, although once again neither target was bright enough for the RGS.

For the extraction of spectra and light curves from the *XMM-Newton* data we used the tools available in the Science Analysis System (SAS[9]), version 6.5.0, with calibration files current to 2005 December 15, and followed the standard protocol as given by the ESA *XMM-Newton* Web site and the ABC guide[10] from the US Guest Observer Facility. In all cases we produced new event list files from the observation data files to incorporate the latest calibration updates and then filtered them with the standard canned expressions. We defined circular source extraction regions (radii of 480 and 360 pixels for the MOS and pn camera, respectively) centered on the centroid of the source, enclosing ~80% of the energy to optimize the signal-to-noise ratio. Simple annular

[9] Available from http://xmm.vilspa.esa.es/external/xmm_sw_cal/sas.shtml.
[10] See http://heasarc.gsfc.nasa.gov/docs/xmm/abc/abc.html.

background-extraction regions were defined on the same central MOS chip for those two cameras; for the pn CCD we used adjacent rectangular regions at similar detector *Y* locations to the target. We also reprocessed the OM data with `omfchain`, extracting light curves using more appropriate (for our relatively faint targets) source aperture and background regions to maximize the signal-to-noise ratio. We also chose binning to match that of the ground-based photometry, and finally, to aid comparison, converted count rates to *B* magnitudes.

The SAS task `evselect` performed the extractions of both X-ray spectra and light curves for source and background. For SDSS J1446+02 and SDSS J2050−05 further time filtering was applied to the event lists prior to spectral extraction to excise intervals of high X-ray background; the revised good time intervals (GTIs) were generated by setting limits on the count rate in hard (>10 keV) light curves for the entire detector. We also restricted acceptable events to singles in the pn CCD (pattern = 0) but up to quadruples in the MOS (pattern $\leq$ 12) to further improve energy resolution. In contrast, in extracting light curves only the standard GTIs were invoked, and we kept both singles and doubles for the pn CCD (pattern $\leq$ 4) to maximize both light curve coverage and signal-to-noise ratio. For SDSS J2101+10 we also restricted the energy range to below 2.5 keV, at which energy the source contributions dominate. SAS tasks `rmfgen`, `arfgen`, and `backscale` generated appropriate redistribution matrix (rmf) and ancillary response files (arf) and calculated the relative scaling of source to background.

The final steps in data reduction used general-purpose utilities in the FTOOLS[11] software suite: `grppha` grouped the spectral bins and associated various files ready for spectral analysis in XSPEC, `lcmath` created background-subtracted light curves and combined the two MOS light curves, while `earth2sun` applied a correction to the time stamps for the solar system barycenter.

2.2. *Optical*

Ground-based photometry was obtained for all three sources using the US Naval Observatory Flagstaff Station (NOFS) 1 m telescope and a 2048 × 2048 CCD. An open filter was used that had close to a *V* response, and the magnitudes were calibrated from separate nights of all-sky photometry with Landolt standards. Light curves were made by using differential photometry with respect to comparison stars in each field and the magnitudes measured using IRAF[12] routines. For SDSS J1446+02, 4 hr of photometry began about 1 hr after the *XMM-Newton* observation ended on 2004 January 30. No data were obtained for the second observation, but an additional 5 hr of photometry from 2003 May 7 was used to establish the optical period. For SDSS J2050−05, 3 hr of photometry were obtained 3 days after the *XMM-Newton* observations, while the 3.5 hr of observations for SDSS J2101+10 took place 5.5 hr prior to the start of *XMM-Newton* coverage. In all cases, the ground-based measurements agreed with the OM in showing the systems were all in their normal state of accretion.

In order to determine the orbital period for SDSS J1446+02, 4 hr of time-resolved spectra were obtained on 2003 April 27. The Double Imaging Spectrograph was used on the 3.5 m telescope of the Apache Point Observatory (APO). Twenty-three 10 minute blue and red spectra were obtained with a 1.″5 slit, covering the regions 4200−5100 and 6300−7200 Å with a resolution of about 2 Å. IRAF routines were used to calibrate the spectra for wavelength and flux using standards from the night. Velocities were measured for the prominent emission lines using the centroid ("e") routine in the IRAF *splot* package; a double-Gaussian method (Shafter 1983) was tried as well. A single spectrum of SDSS J2101+10 was also obtained at APO five nights before the *XMM-Newton* observation. The Balmer and He II strengths are very similar to the SDSS spectrum shown in Szkody et al. (2003a).

Circular spectropolarimetry was also performed for the three systems in a search for evidence of magnetic fields. The CCD spectropolarimeter SPOL was used (Schmidt et al. 1992) on the Steward Observatory (SO) 2.3 m Bok telescope and the 6.5 m MMT, as indicated in Table 1. All measurements of SDSS J1446+02 and SDSS J2101+10, and two of the three on SDSS J2050−05, yielded spectrum-averaged values $|v| = |V/I| < 0.4\%$. Each result is well within 3 σ of zero and thus consistent with being unpolarized. However, a third epoch on SDSS J2050−05, obtained on 2003 May 29 in good observing conditions at the MMT, yielded $|v| = +1.06\%$. The signal-to-noise ratio of these data is sufficient to reveal that the circular polarization rises continuously from $v \sim 0$ at ~4200 Å to $v \sim 3\%$ beyond $\lambda = 8000$ Å. This and other evidence for polarization by cyclotron emission in SDSS J2050−05 is discussed in § 4.2.

3. ANALYSIS AND RESULTS

3.1. *X-Ray Spectral Fitting*

The extracted spectra were binned at >20 counts bin^{-1}, to facilitate the use of χ^2 statistics to find the best model fits. For all sources the background contributed less than 3% of the flux within the source aperture; hence, simpler fitting of background-subtracted spectra was deemed acceptable. At the very lowest energies the calibration of the EPIC detectors remains uncertain; following the latest guidelines, we restricted our fitting to >0.2 keV for the MOS and >0.15 keV for the pn CCD. In every case, we performed joint fits to the data from all three X-ray cameras simultaneously, where all model parameters were fixed apart from the relative normalization of the pn CCD relative to the MOS (which were assumed to be identical). In the cases for which we separated the data into two phase or time bins we then had six data sets. Starting from the case for which all relative normalizations, as well as other model parameters, were kept constant, we then allowed normalizations (but keeping the MOS-to-pn ratios constant) and then other model parameters like temperature to vary, *F*-testing to see whether the additional degrees of freedom were statistically warranted each time. The best fits that we present in figures and tables are those in which the model has the fewest free parameters (i.e., leaves the most degrees of freedom); any further freeing of parameters did not then significantly reduce the (reduced) χ^2 values.

Furthermore, in finding the best-fit models we always started from the simplest single-emission component, solely absorbed by interstellar dust, with an initial value for $N_{\rm H}$ as predicted by dust maps for the appropriate line of sight through the Galaxy. Typically, we used a single bremsstrahlung model or a model including explicit line emission (the XSPEC model MEKAL) as expected for the optically thin thermally emitting plasma encountered in CVs. In all cases, these simplest models failed to provide a good fit; hence, we moved onto a variety of more complex combinations, e.g., multitemperature or two-temperature thermal plasmas, additional soft blackbody components (as emitted by the heated polar caps in polars), and the effects of local partial

[11] Available from http://heasarc.gsfc.nasa.gov/lheasoft/ftools/.

[12] IRAF (Image Reduction and Analysis Facility) is distributed by the National Optical Astronomy Observatory, which is operated by the Association of Universities for Research in Astronomy, Inc., under cooperative agreement with the National Science Foundation.

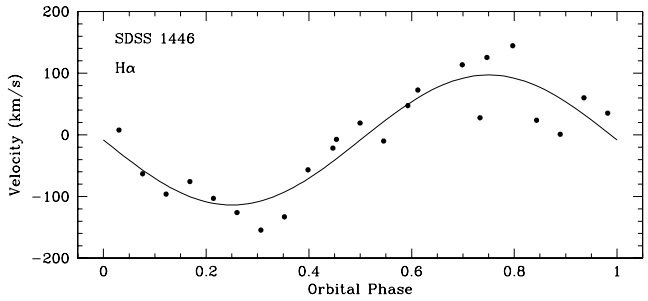

FIG. 1.—Radial velocities for the Hα emission line in SDSS J1446+02, phase-folded on the best-fit period, $P = 3.8 \pm 0.3$ hr. Overplotted is the sinusoid fit with $K = 105 \pm 11$ km s^{-1} and $\gamma = -8 \pm 5$ km s^{-1}.

covering absorption (i.e., due to obscuration by the accretion stream and/or curtain). We discuss the details of the best fits as we report the results of our various analyses for each target in turn.

3.2. *SDSS J1446+02*

3.2.1. *Search for Periodicities*

From our APO spectroscopy run on SDSS J1446+02 we generated radial velocity curves for the prominent emission lines. A least-squares sine fit to the velocities was then used to determine the systemic velocity, the semiamplitude, the orbital period, and the phase (based on the red-to-blue crossing). While the Hα, Hβ, Hγ, and He II lines were all measured, there were large deviations with respect to the best-fit sine wave in all cases (total σ of the fit of 34, 46, 75, and 73 km s^{-1}, respectively); hence, we only consider the fit to the Hα curve in any detail (shown in Fig. 1). All lines gave a period solution near 4 hr, which is very close to the length of the data set. The Hα solution shown in Figure 1 is for a period of 3.8 ± 0.3 hr, $K = 105 \pm 11$ km s^{-1}, and γ of -8 ± 5 km s^{-1}, with red-to-blue crossing (phase 0) at 7:30 UT on 2003 April 27. Because the period is so close to the length of the observation, it is not a robust determination, but useful in showing that the orbital period is not short (i.e., under 2 hr).

For SDSS J1446+02 we also possess four optical light curves (two from the ground and two from the OM) plus those from the EPIC X-ray cameras. To maximize the signal-to-noise ratio we summed the results from the two MOSs; however, since these are always of longer duration than the pn CCD, we did not combine pn and MOS data at this stage. We performed a Lomb-Scargle periodogram (Scargle 1982) analysis of each of our light curves. In every case a significant peak was found at a period of 49 minutes, which we identify as the spin period of the white dwarf. In addition, longer term variations were apparent in the optical light curves, with peaks corresponding to around 4 hr, close to the signal found in the time-resolved APO spectra. To determine the periods most accurately we used sinusoidal fitting to the longest 2003 May 7 NOFS light curve, with a sinusoid–plus–first harmonic model for the pulse and a simple sinusoid for the longer period variation. This yielded a period of 0.0338 ± 0.004 days (48.7 ± 0.5 minutes) for the pulse and 0.165 ± 0.015 days (4.0 ± 0.4 hr) for the longer period, which we presume to be the orbital period of the system. Once again we caution that the 2003 May curve provides only 1.3 cycles coverage of our tentative orbital period, and it remains poorly constrained. Nevertheless, we then fitted the other three optical curves with sinusoids constrained to the pulse and orbital periods and subtracted the latter. In Figure 2 we show the two resulting NOFS light curves; the pulse profile is obvious in most cycles in the 2003 May curve, whereas in 2004

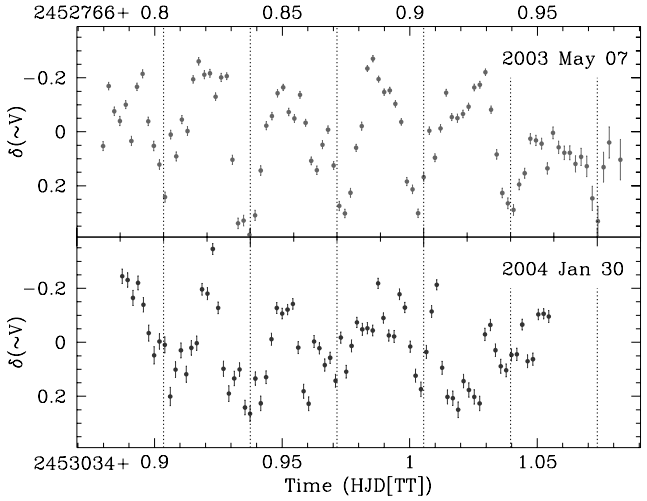

FIG. 2.—NOFS $\sim V$ light curves from the two different observations of SDSS J1446+02 plotted using a common time scaling. We also overplot vertical bars to mark the length of each spin cycle; comparison of the variations during each successive spin cycle shows how much more regular they are on 2003 May 7 than on 2004 January 30. Possibly enhanced flickering is responsible for the increased scatter in the latter curve.

January there is far more scatter, especially away from minimum light. This may simply be due to varying amounts of flickering, perhaps indicative of small changes in accretion state. Lastly, we phase-folded (and binned) the light curves on the pulse period to examine its profile in greater detail. The binned results are shown (along with the X-ray) in Figure 3. The profile is clearly far from sinusoidal, having a relatively broad and flat-topped peak and a narrower V-shaped minimum.

Before phase-folding the X-ray data we created five different energy-selected light curves in order to investigate any dependence of the pulse profile on energy. The final binned light curves shown in Figure 3 were constructed by summing the folded and binned results for all three X-ray cameras to maximize the signal-to-noise ratio. Perhaps not too surprisingly the profile of the X-ray pulse is very different from the optical, but it is noteworthy that the X-ray and optical are neither in phase nor antiphased. Instead, the peak of the X-ray roughly leads that of the optical by $\sim$0.3 in phase. The X-ray pulse is also energy-dependent, with the largest amplitude (and symmetrical peaked pulse) in the two lowest energy bins; the amplitude then decreases with energy, until above 5 keV there is no significant variation.

3.2.2. *Spectral Variations with Phase*

The variation in pulse amplitude with energy is exactly that which we would expect if obscuration by a local absorber is responsible. In fitting the X-ray spectra we first found a fit to the entire data set, but then applied this model separately to spectra phase-selected from the maximum ($\phi = 0.05$–0.55) and minimum ($\phi = 0.55$–1.05) flux intervals of the pulse profile. The details of the fits are given in Table 2. The model that has the best fit consists of a two-temperature thermal plasma (MEKAL), absorbed by a small Galactic column and also by a much larger variable partial-covering absorber. The fit to the combined spectrum achieved a barely acceptable reduced $\chi^2 = 1.1$ for 134 degrees of freedom, although it does better than any other model. This model has a well-constrained cool plasma of $kT = 130^{+2}_{-4}$ eV contributing unresolved soft emission-line structure plus a very hot component whose temperature pegged at 80 keV, the upper limit for the MEKAL model. Furthermore, the values of the Galactic and local columns were very poorly constrained. This is

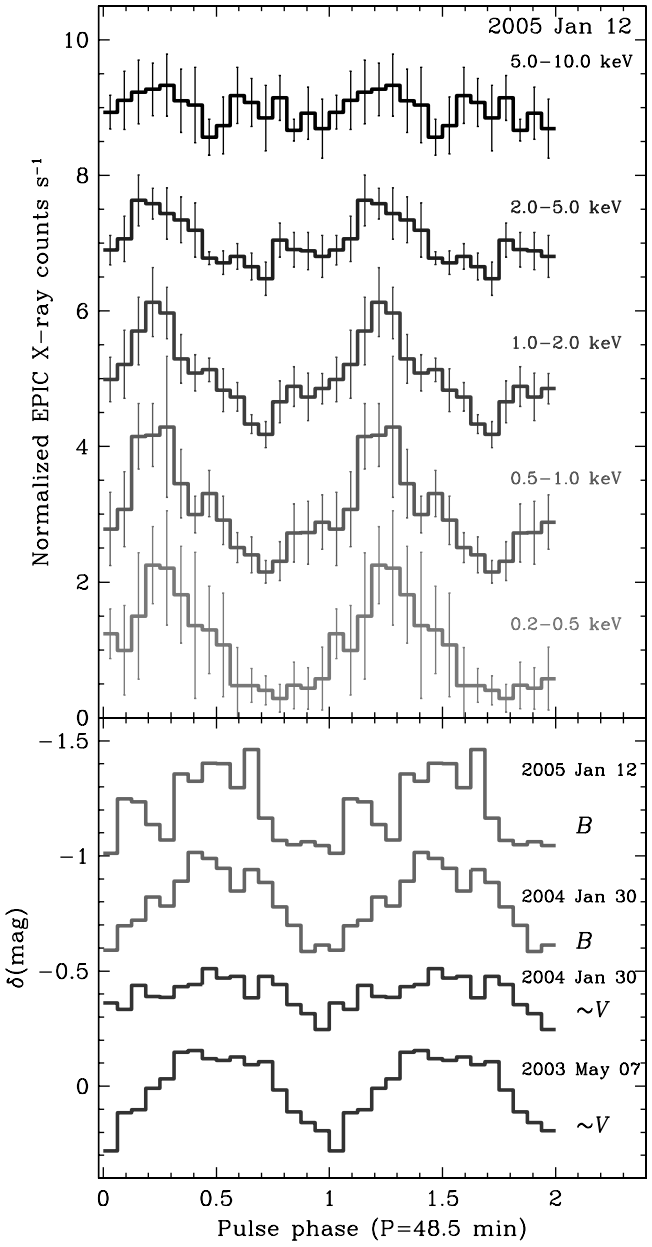

FIG. 3.— White dwarf spin-phase folded and binned light curves for SDSS J1446+02. *Top*: Energy-selected EPIC X-ray light curves; note the marked change in amplitude, increasing with decreasing energy. *Bottom*: Optical light curves from the two *XMM-Newton* OM (in *B*) and two NOFS observations (in an approximate *V* band); in the NOFS light curves the change in amplitude, due to the variation in scatter about the mean curve, is made very apparent. Note that (1) the simultaneous X-ray and OM 2005 January 12 light curves share a common ephemeris, arbitrarily chosen to place optical minimum at phase = 0.0, and the phasing of each of the other optical light curves has simply been chosen to align their optical minima, and that (2) for clarity each of these light curves has been offset vertically, with 2 normalized X-ray counts and 0.4 mag, respectively.

probably an effect of trying to fit a highly phase-variable spectrum with a single model (even this fairly complex one). Indeed, after separating the data into "max" and "min" subsets, a joint fit to these spectra was a significant improvement (see Fig. 4). There was not a significant change in the reduced χ^2, but we were then able to find well-constrained values for the absorbing columns and a physically plausible temperature for the hottest MEKAL component of $kT = 58^{+22}_{-19}$ keV. Once again the fit required a very cool MEKAL model to account for line structure in the 0.3–0.4 keV range, plus O VII emission at 0.56 keV; indeed, this parameter is now pegged at its minimum value of 81 eV, indicating that some problems still remain (but the need for a very cool plasma is less problematic than an unphysically hot one, given the physical conditions in the expected complex multitemperature accretion column). In this fit the partial-covering absorber parameters for the max tended to zero; hence, we fixed them as such; the min interval as expected requires a thick column around 4×10^{22} cm^{-2}, with a 61% covering fraction. In our joint fit we found no statistical support for varying any of the normalization parameters; the change between max and min is entirely accounted for by the introduction of the thick partial-covering absorber. Therefore, the fully unabsorbed flux (0.01–10 keV) remains constant at 3×10^{-11} ergs cm^{-2} s^{-1}, whereas the effect of the absorption leads to clear energy-dependent changes in the observed fluxes: a drop of 60% (4.6×10^{-13}–1.8×10^{-13} ergs cm^{-2} s^{-1}) in the softest 0.2–2.0 keV band, a decrease of only 30% (7.6×10^{-13} to 5.6×10^{-13} ergs cm^{-2} s^{-1}) in the 2.0–5.0 keV band, and no significant change in the flux above 5 keV.

3.3. *SDSS J2050−05*

The eclipses seen in the optical photometry of Woudt et al. (2004) are also very apparent in the X-ray light curves and in our *B*-band OM results. Their ephemeris is sufficiently precise that there is merely a 0.01 cycle uncertainty at the time of our *XMM-Newton* observations. Adding our own eclipse-center measurements, we are able to even further refine the ephemeris to

$$\mathrm{HJD_{min}(TT)} = 2{,}453{,}296.29816(6) + 0.06542463(1)E \text{ days},$$

where the numbers in parentheses indicate the 1 σ uncertainty in the last digit. Also, note that the time is given in Terrestrial time (UT = TT + 64.184 s at the present epoch).

Besides the eclipses, the X-ray light curves exhibit large amplitude but apparently irregular flaring behavior. We divided the X-ray data into two energy bins, above and below 1.6 keV, roughly encompassing the same count rates, then phase-folded the light curves; we plot them in Figure 5, where we also plot each cycle of data with a different symbol. Although this energy division is not physically motivated, it does roughly separate the energies severely affected by photoelectric absorption from those little affected (as can been seen in Fig. 6). We note, however, that the soft band does include contributions from physically distinct X-ray emission regions (the heated white dwarf surface and the accretion column), which should be borne in mind in any interpretations of the light curves. We see that the flaring does not repeat in each orbit, and that it is far more significant below 1.6 keV. The overplotted binned data (*stepped line*) bring out the average orbital modulations more clearly. At the higher energies there appears to be a broad peak, cut unevenly by the eclipse, whereas at lower energies the rise in flux to peak does not occur until phase 0. As we did for SDSS J1446+02, we undertook X-ray spectral fitting to both the complete data set, and two phase-selected intervals, here dubbed "peak" and "trough," excluding the eclipse phase; these regions are also indicated in Fig. 5.

For the complete data set acceptable fits (see Table 3) were found for two-component models with Galactic absorption consistent with the maximum line-of-sight column, with an optically thin thermal component (hot bremsstrahlung or MEKAL plasma equally) plus a soft blackbody. However, the temperature of the hotter component at ~80 keV is higher than typically found in CVs. We then investigated the phase-selected spectra seeking a single model requiring the fewest varying parameters. The final model consists of a two-temperature thermal component plus a

TABLE 2
X-Ray Spectral Fits for SDSS J1446+02

Model	Reduced χ^2	Degrees of Freedom	N_H ($\times 10^{20}$ cm^{-2})	Partial Covering		Emission Model Parameters
				N_H ($\times 10^{22}$ cm^{-2})	Fraction	
Bremsstrahlung	1.5	139	6.4[a]	...	...	$kT = 200$ (pegged)
Power law	1.11	136	$1.4^{+0.8}_{-1.0}$	0.8 ± 0.2	$0.41^{+0.04}_{-0.07}$	$\Gamma = 1.2 \pm 0.2$
Multi-T MEKAL[b]	1.14	137	1.6 ± 0.7	1.3 ± 0.2	0.64 ± 0.02	$kT_{max} = 60$ keV (fixed[c]), $\alpha = 1.0$ (fixed)
2 T MEKAL	1.10	134	4^{+27}_{-2}	$0.9^{+3.9}_{-0.2}$	$0.47^{+0.05}_{-0.04}$	$kT_1 = 130^{+2}_{-4}$ eV, $kT_2 = 80^{+0}_{-19}$ keV
2 T MEKAL[d]	1.08	104	13^{+2}_{-3}	None (max), $4.4^{+1.6}_{-0.8}$ (min)	None (max), 0.61 ± 0.03 (min)	$kT_1 = 81^{+4}_{-0}$ eV, $kT_2 = 58^{+22}_{-19}$ keV

[a] This fit did not converge well; hence, no error estimates are available.
[b] We used the XSPEC model CEMEKL, in which a fine grid of MEKAL models are co-added, with the emission measures following a power law in temperature with index α and up to kT_{max}; i.e., normalizations scale as $(T/T_{max})^{\alpha}$.
[c] Here, kT_{max} was fixed to a plausible value; free fit does not converge.
[d] Joint fit to phase-selected maximum and minimum flux intervals.

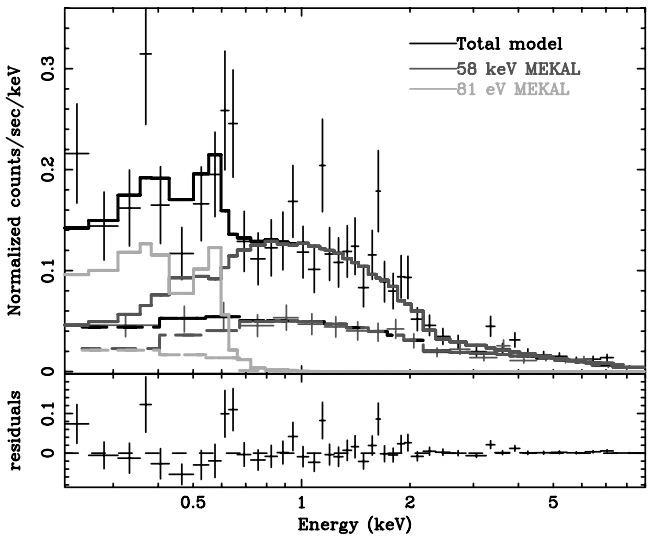

FIG. 4.— *Top*: *XMM-Newton* EPIC-pn CCD spectra for SDSS J1446+02 from the maximum (*black data points [with error bars]*) and minimum (*dark gray data points [with error bars]*) spin-phase intervals; the MOS data, used in the full joint fits, have been omitted for clarity. The best-fit two-temperature MEKAL model is overplotted for each (*solid and dashed lines, respectively*); we also plot the two-component contributions. *Bottom*: Residuals to the fit of the total model. [*See the electronic edition of the Journal for a color version of this figure*.]

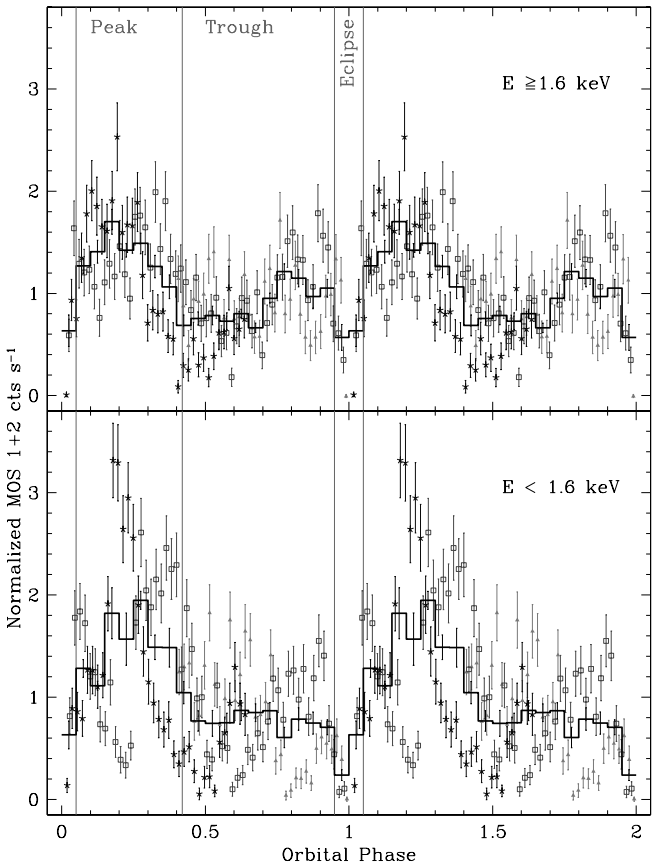

FIG. 5.— Energy-selected *XMM-Newton* EPIC-MOS (combined) X-ray light curves of SDSS J2050−05, phase-folded on our revised ephemeris: *top*, hard band with $E \geq 1.6$ keV; *bottom*, soft band with $E < 1.6$ keV. Each of the three cycles covered is shown with a different symbol and gray shade, in order to show how much of the variability is apparently random flickering, and is more pronounced in the soft energy band. The average orbital modulation is brought out by binning the data; this curve is overplotted in solid black. The vertical gray bars and labeling indicate the three phase intervals into which the data were subdivided to study variations in the spectra. [*See the electronic edition of the Journal for a color version of this figure*.]

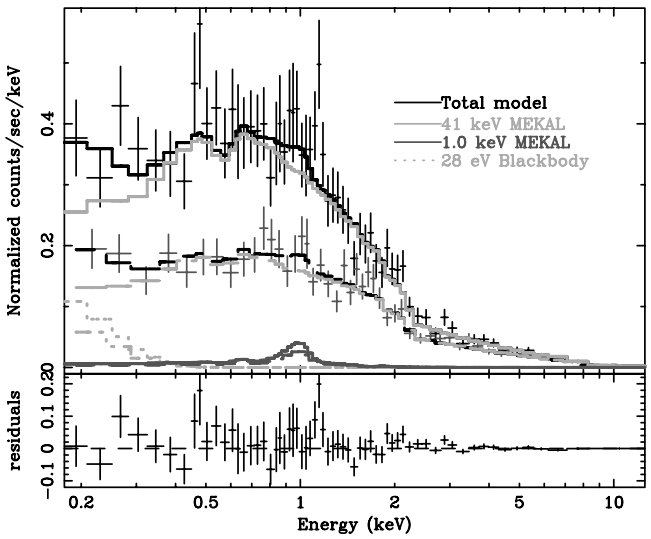

FIG. 6.— *Top*: *XMM-Newton* EPIC-pn CCD spectra for SDSS J2050−05 from the peak (*black data points [with error bars]*) and trough (*dark gray data points [with error bars]*) orbital phase intervals; the MOS data, used in the full joint fits, have been omitted for clarity. The best-fit two-temperature MEKAL plasma plus blackbody model is overplotted for each (*solid and dashed lines*, *respectively*); we also plot the various component contributions. The hotter emitting gas provides the dominant contribution, and the change in overall flux between the intervals is due to a combination of its changing normalization and the extra absorption from a dense partial covering component. *Bottom*: Residuals to the fit of the total model. [*See the electronic edition of the Journal for a color version of this figure*.]

soft blackbody with partial covering absorption. In the light of this success we also fitted the complete data set with the same model; in all cases we found physically plausible temperatures and absorption columns. The dominant contribution to the observed absorbed flux (98% in the 0.01–10 keV range) is from a hot MEKAL with $kT \approx 40$ keV, but *F*-tests confirm the importance of the soft blackbody to provide the softest X-ray flux (at 93% confidence) and the cool MEKAL to account for significant unresolved line emission at ~1 keV (98%). The change in the spectrum from peak to trough is in part due to increased partial covering absorption—the peak spectrum requires no absorption in excess of the Galactic column, while for the trough we find a 35% covering column with $N_{\rm H} = 1.3 \times 10^{22}$ cm^{-2}—and also to a decrease by 25% in the normalization of the hot MEKAL plasma; the blackbody and cool MEKAL normalizations remain unchanged. The fully unabsorbed 0.01–10 keV flux amounts to 5×10^{-12} ergs cm^{-2} s^{-1}, with 40% contributed by the soft blackbody. In Figure 6 we show the fits to the phase-selected spectra, together with a breakdown of the three components; for clarity we only show data from the pn CCD, although we used the pn CCD and the two MOS spectra when fitting.

3.4. *SDSS J2101+10*

With no previously known periods, either spin or orbital, our first step was to examine the light curves (see Fig. 7) for periodicities. Unfortunately, the *XMM-Newton* data span only ~1.5 hr, and even the NOFS light curve is only 3.5 hr long, limiting our sensitivity to any modulations with periods much in excess of 2 hr. Moreover, the variability in both X-ray and optical bands appears extremely complex. The longest curve, the NOFS optical, appears to show two distinct humps at around 0.87 and 0.94 [truncated HJD(TT)], but of course even here only two cycles are present. Running a phase dispersion minimization (PDM; Stellingwerf 1978) period-folding search on this light curve we find three signals, but the lowest frequency one is close to the

TABLE 3

X-Ray Spectral Fits for SDSS J2050−05

				Partial Covering			
Model	Reduced χ^2	Degrees of Freedom	$N_{\rm H}$ ($\times 10^{20}$ cm^{-2})	$N_{\rm H}$ ($\times 10^{22}$ cm^{-2})	Fraction	$kT_{\rm BB}$ (eV)	kT (keV)
Bremsstrahlung	0.99	418	4.3 ± 0.3	...	...	...	166^{+33}_{-40}
MEKAL	1.01	418	4.8 ± 0.3	...	...	...	80^{+0}_{-5}
2 T MEKAL	1.00	416	7.4 ± 0.3	...	...	...	$(8.08^{+0.1}_{-0}) \times 10^{-2}$, 80^{+0}_{-17}
BB + MEKAL	0.99	416	$5.7^{+0.5}_{-0.4}$	...	...	20^{+8}_{-6}	80^{+0}_{-9}
BB + bremsstrahlung.....	0.98	416	$5.6^{+0.4}_{-0.8}$	...	...	22^{+1}_{-10}	100^{+32}_{-19}
2 T MEKAL + BB	0.99	412	$5.1^{+0.5}_{-0.7}$	$1.4^{+0.8}_{-0.6}$	$0.14^{+0.45}_{-0.05}$	32^{+1}_{-5}	$1.3^{+1.3}_{-0.5}$, 59^{+21}_{-15}
2 T MEKAL + BB[a].....	0.88	417	$4.9^{+0.5}_{-0.7}$	None (peak), $1.3^{+0.4}_{-0.3}$ (trough)	None (peak), 0.35 ± 0.03 (trough)	28^{+10}_{-13}	$1.0^{+0.3}_{-0.2}$, 41^{+5}_{-13}

[a] Joint fit to phase-selected peak and trough intervals.

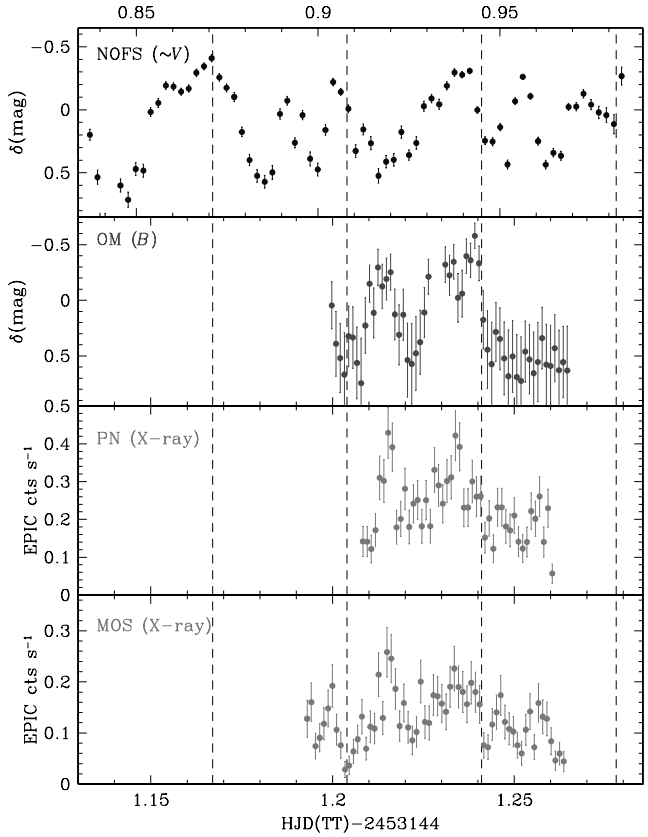

FIG. 7.—Light curves for SDSS J2101+10 from NOFS (optical) and *XMM-Newton* (optical and X-ray). The lower three panels share a common time axis, while the earlier NOFS observation differs and is marked on the top axis. The vertical bars mark the times of (arbitrary) phase 0.0 and 0.5 for a 107 minute period (detected in the NOFS light curve).

inverse of the data time span and is therefore unreliable. This leaves minima at around 13.5 days^{-1} (107 minutes) and 26.4 days^{-1} (55 minutes), which are close to being harmonically related to each other. In Figure 8 we show the PDM for the NOFS light curve and the light curve folded on the two candidate periodicities. The fold on the longer period confirms the repeatability of the aforementioned humps; only at phases (arbitrary) 0.25–0.5 do the two cycles agree. However, the fold is also somewhat double-humped, with possibly a second interval of higher flux at around 0.9, although here there is a large amount of scatter. Folding on 54 minutes, the points line up along an approximately sinusoidal curve, but again there is significant scatter about this mean at all phases. Furthermore, for this shorter period we can usefully interrogate the OM and MOS light curves; their PDMs are also plotted in Figure 8. No strong signals appear around 54 minutes.

Returning to Figure 7, in order to consider the NOFS periods further we have overplotted vertical bars to mark phase 0.0 and 0.5 of a 107 minute period, arranging the time axes for the *XMM-Newton* and NOFS observations to yield phase agreement (only four cycles elapse between the two sets of observations). We see that the repeatable NOFS humps agree in phase and approximate form with a hump in the OM light curve. However, at other phases agreement is lost; in particular, another peak precedes the major hump in the OM curve, possibly correlated with a similar X-ray peak, in fact. Ignoring the high-frequency flickering in the X-ray light curves, there is possibly a slower variation on the ~100 minute timescale, although of course we have no way to test whether this behavior actually repeats.

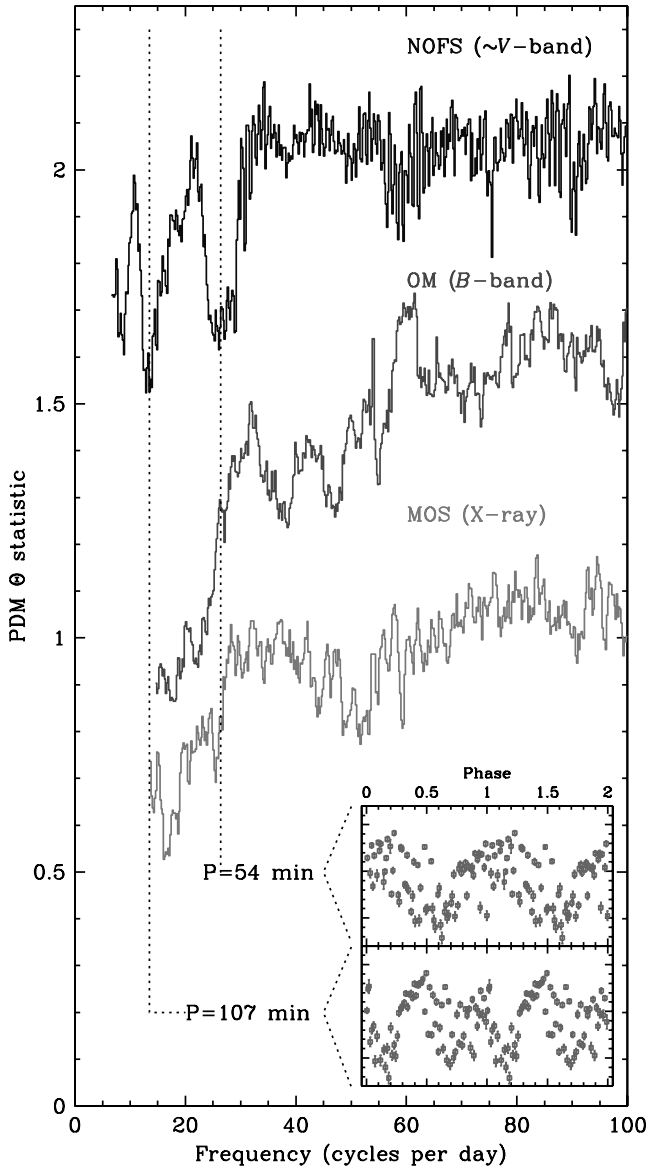

FIG. 8.—PDM periodograms for the MOS X-ray and NOFS and OM optical light curves of SDSS J2101+10. The successive curves have been offset vertically by 0.5 for clarity and have been truncated at the low-frequency end at the inverse of the respective light-curve time span. The inset shows the NOFS light curve folded into its candidate periods, 54 and 107 minutes. The ordinate is in relative *V* magnitudes, with a 0.5 mag interval between large tick marks.

In the absence of any decisive periods, we simply fitted models to the complete X-ray spectrum. These are detailed in Table 4. A range of emission components from a single fairly cool MEKAL model ($kT = 9$ keV) to a multitemperature version with $kT_{\max} = 25$ keV provide adequate fits, all with a single absorbing component with $N_{\rm H} \approx 8 \times 10^{20}$ cm^{-2}, consistent with the Galactic line-of-sight maximum. An example fit to the spectra is shown in Figure 9; the resulting unabsorbed 0.01–10 keV flux is 1.7×10^{-12} ergs cm^{-2} s^{-1}.

4. CLASSIFYING THE THREE SOURCES

4.1. *Nature of SDSS J1446+02*

All the observational evidence indicates that SDSS J1446+02 is a short-period IP. A classic signature of IPs is the presence of multiple periodicities in their light curves. For SDSS J1446+02 we find that both its optical and X-ray fluxes are strongly modulated

TABLE 4
X-Ray Spectral Fits for SDSS J2101+10

Model	Reduced χ^2	Degrees of Freedom	$N_{\rm H}$ ($\times 10^{20}$cm^{-2})	kT_1 or $kT_{\rm max}$ (keV)	kT_2 (keV) or α
MEKAL	0.82	95	7.1 (fixed)[a]	9 ± 1	...
MEKAL	0.80	94	$8.4^{+1.4}_{-0.7}$	8 ± 2	...
2 T MEKAL	0.77	92	$8.6^{+1.2}_{-1.1}$	$9.5^{+3.2}_{-1.6}$	1.0 ± 0.2
Multi-T MEKAL	0.75	93	$8.6^{+1.4}_{-0.9}$	25^{+4}_{-5}	$1.2^{+0.4}_{-0.2}$

[a] The absorbing column is fixed to that estimated from dust maps, given by the FTOOL nH.

at a short 49 minute period, and there is evidence for an additional optical modulation at 4 hr. This latter periodicity also appears in the Hα radial velocity curve. However, more extensive photometric and spectroscopic runs are needed to confirm these, and hence secure the determination of the orbital period. The identification of the 49 minute modulation with the spin period of an asynchronously rotating white dwarf is much more secure: the characteristic energy dependence of the X-ray flux modulation and our simple phase-selected spectral fitting confirm that the variation in flux is dominated by changes in the local absorbing column. This is exactly as seen in many other IPs, as a result of the extended accretion curtain intersecting our line of sight to the X-ray-emitting accretion column.

The underlying X-ray emission can be fitted with that emitted by a two-temperature optically thin plasma, i.e., bremsstrahlung. No doubt this simple model only approximates what must be a complex multitemperature shock region in the accretion column. However, the hotter component with $kT \approx 60$ keV indicates the upper limit to the temperatures therein; again, this value is typical of IPs.

Assuming that $P_{\rm orb} = 4$ hr, we find a ratio of $P_{\rm spin}/P_{\rm orb} = 0.2$, placing SDSS J1446+02 well within the group of so-called conventional IPs, as defined by $0.25 > P_{\rm spin}/P_{\rm orb} > 0.01$ and $P_{\rm orb} > 4$ hr (Norton et al. 2004). In all respects the observed properties of SDSS J1446+02 are consistent with a garden-variety IP.

4.2. *Nature of SDSS J2050−05*

The observational evidence favors a polar classification for SDSS J2050−05. One spectropolarimetric observation found significant circular polarization that increases to $v \sim 3\%$ for $\lambda >$ 8000 Å. This result suggests that the strongest cyclotron harmonics may lie in the near-IR, and thus that the magnetic field is relatively low, $B \lesssim 30$ MG, or that the specific accretion rate in the cyclotron-emitting portions of the funnel(s) is relatively low, $\dot{m} \lesssim 1$ g cm^{-2}, or both. No cyclotron harmonics are evident in either the total flux or circular polarization spectra, consistent with a high temperature shock. Therefore, SDSS J2050−05 is probably not a low accretion rate polar (Schwope et al. 2002; Szkody et al. 2003b; Schmidt et al. 2005), for which mass-transfer appears to occur not via Roche-lobe overflow but rather by efficient magnetic capture of the secondary star's stellar wind.

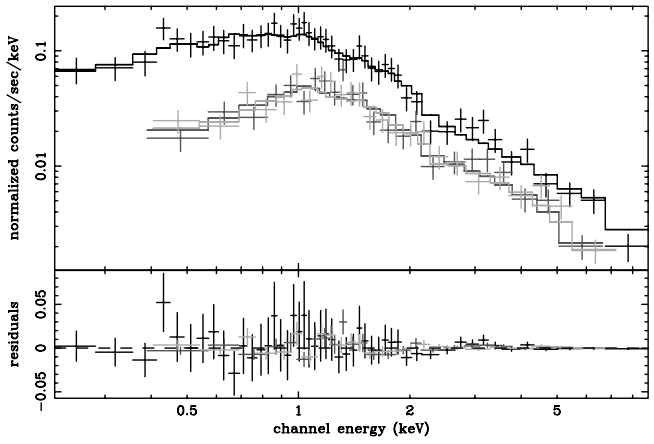

Fig. 9.—*XMM-Newton* EPIC spectra (*data points*) and best-fit model (*line*) for SDSS J2101+10: *black*, pn CCD; *dark gray*, MOS1; *light gray*, MOS2. This model consists of a multitemperature optically thin plasma model (CEMEKL) absorbed by $N_{\rm H} = 7.5 \times 10^{19}$ cm^{-2}. In the bottom panel the residuals to the fit are plotted.

In support of the above interpretation the X-ray spectra of SDSS J2050−05 are fitted well by a two-temperature thermal plasma model (MEKAL), but, in addition, the data require a soft blackbody component. In this case, the two MEKAL components have temperatures of 1 and 41 keV respectively, once again likely indicating the limits of the range of temperatures present in the optically thin emitting plasma, both quite typical for polars. The blackbody has a temperature of about 30 eV, again within the observed range for polars. In the peak region, this cool blackbody component, arising from the heated surface of the white dwarf, contributes about 40% of the unabsorbed 0.01–10 keV flux. In terms of the energy balance, assuming an X-ray albedo for the white dwarf surface of $a_{\rm X} = 0.3$ and that the cyclotron contribution to the energy losses is negligible, one finds $L_{\rm BB}/L_{\rm br} \approx \pi f_{\rm BB}(1 - a_{\rm X})d^2/2\pi f_{\rm br}(1 + a_{\rm X})d^2 \approx 0.2$, which, given the uncertainties in estimating the unabsorbed soft flux, is comparable to recent measures of the energy balance in other actively accreting polars.

As an eclipsing system, the orbital period is very well established. In the X-ray light curves we again see eclipses, but the remainder of the variability is complex. It is dominated by aperiodic flickering behavior, which is strongest in the softer X-ray flux (below 1.6 keV). In an attempt to discover any underlying modulation in the orbital period, we created phase-binned light curves averaged over the three cycles of data. What remains appears quite typical of a polar, in which one accretion pole is always visible (i.e., no white dwarf self-eclipse). This produces emission modulated on the orbitally synchronized white dwarf spin period, since the projected area of the emitting region changes with phase. The fact that only the normalization of the hotter thermal emission component appears to vary between peak and trough spectra is probably simply owing to poor statistics for the much smaller contributions from the cooler MEKAL plasma and soft blackbody components. The shape of the average, noneclipse harder X-ray ($E > 1.6$ keV) light curve is indeed approximately sinusoidal, whereas in the soft band the light curve does not rise until after the eclipse, i.e., its flux remains low in the phase range $\phi \approx 0.7$–0.95. The energy dependence of this feature suggests that photoelectric absorption may be the cause. Indeed, the spectrum for the $\phi \approx 0.4$–0.95 trough phase interval does require a fairly high column, which partially covers the X-ray emission.

Such preeclipse energy-dependent dipping structure is seen in many other eclipsing polars, e.g., EP Dra, HU Aqr, and UZ For (Ramsay et al. 2004; Schwope et al. 2001; Sirk & Howell 1998). In the high-quality soft X-ray light curves of HU Aqr there is one broad dip centered on phase 0.7 and a narrower feature at around 0.9. These are interpreted as arising from the accretion column obscuring the nearby heated photosphere of the white dwarf, while the more distant accretion stream accounts for the sharper dip; indeed, the width and azimuth of this dip can be related to the geometry of the region where the stream threads onto the white dwarf's magnetic field. Unfortunately, given the quality of our own data (both lacking the high signal-to-noise ratio and afflicted by the flaring), we cannot identify the dipping components and hence cannot probe the accretion flow in greater detail. Of course, from our spectral fitting we know that the soft flux arises from both the white dwarf and various parts of the accretion column, which would further complicate a more detailed analysis.

4.3. *Nature of SDSS J2101+10*

Although originally identified as a candidate mCV, given the strength of its high-excitation optical emission lines the follow-up observations of SDSS J2101+10 we have presented do not seem to confirm this classification. We find no strong modulation of its X-ray flux, quite unlike any polar (e.g., SDSS J2050−05). The X-ray spectrum also does not require any absorption in excess of the estimated Galactic column, effectively ruling out a typical IP. The X-ray emission is describable by a variety of thermal plasma (MEKAL) models, although with a noticeably lower maximum temperature ($kT \approx 10$, or at most 25, keV) than is found in most mCVs or, indeed, in our fits to SDSS J1446+02 or SDSS J2050−05. This cooler plasma is in fact far more typical of disk-accreting systems. Only the SW Sex stars show He II with strength comparable to the magnetics; both the lack of absorption in the line profiles and their barely detectable radial velocities could be accounted for by a low inclination to our line of sight.

5. CONCLUSIONS

We have reported on observations allowing classification of three new SDSS CVs showing prominent He II: SDSS J1446+02, SDSS J2050−05, and SDSS J2101+10. Each represents a different class of CV, known to exhibit such high-excitation emission lines.

SDSS J1446+02 is a clear example of an IP. We find two periodicities at about 4 hr and 49 minutes, arising respectively from the orbit and the asynchronously spinning white dwarf. The X-ray spectrum comprises a multitemperature thermal plasma, with a maximum of 60 keV, modulated by phase-dependent local absorption. This likely originates from obscuration by the accretion curtains formed by the accreting material as it flows between the disrupted disk and the magnetic poles of the white dwarf.

SDSS J2050−05 represents the most highly magnetized of the three, a fully spin-orbit synchronized polar, with an orbital period of 1.57 hr. In this case no disk forms, and all accretion is channeled along the field lines to a single dominant pole. Owing to its high inclination, there is a phase interval when the accretion stream obscures the X-ray emitting region, but most of the modulation on the spin/orbit appears consistent with simply its changing aspect. The X-ray emission has two components. The dominant one is characteristic of the postshock bremsstrahlung-cooled optically thin plasma of the accretion column, here with temperatures ranging from 1 to 40 keV; this also heats the surface of the white dwarf, leading to additional soft blackbody (30 eV) emission.

In SDSS J2101+10 we suggest that the combination of high accretion rate and lower magnetic field strength allows disk-mediated accretion but also the formation of He II emission lines in the optical spectra; i.e., if it were at higher inclination it would appear as a classic SW Sex star. Its X-ray spectra indicate a rather cool thermal plasma ($\sim$10 keV) more typical of disk systems and an unobscured line of sight, inconsistent with an IP. From only weak modulation of its X-ray and optical light curves (unlike a polar) we suggest an orbital period in the 100 minute range.

The authors wish to thank the anonymous referee for their thorough review and useful comments that helped improve the paper. This work was supported by *XMM-Newton* grant NNGO4GG66G to the University of Washington and is based on observations obtained with *XMM-Newton*, an ESA science mission with instruments and contributions directly funded by ESA Member States and the USA (NASA). G. S. acknowledges the support of NSF grant AST 03-06080, and P. S. AST 02-05875.

Funding for the SDSS and SDSS-II has been provided by the Alfred P. Sloan Foundation, the Participating Institutions, the National Science Foundation, the US Department of Energy, the National Aeronautics and Space Administration, the Japanese Monbukagakusho, the Max Planck Society, and the Higher Education Funding Council for England. The SDSS Web site is http://www.sdss.org.

The SDSS is managed by the Astrophysical Research Consortium for the Participating Institutions. The Participating Institutions are the American Museum of Natural History, Astrophysical Institute Potsdam, University of Basel, Cambridge University, Case Western Reserve University, the University of Chicago, Drexel University, Fermilab, the Institute for Advanced Study, the Japan Participation Group, Johns Hopkins University, the Joint Institute for Nuclear Astrophysics, the Kavli Institute for Particle Astrophysics and Cosmology, the Korean Scientist Group, the Chinese Academy of Sciences (LAMOST), Los Alamos National Laboratory, the Max Planck Institute for Astronomy (MPIA), the Max Planck Institute for Astrophysics (MPA), New Mexico State University, Ohio State University, the University of Pittsburgh, the University of Portsmouth, Princeton University, the United States Naval Observatory, and the University of Washington.

REFERENCES

den Herder, J. W., et al. 2001, A&A, 365, L7
Norton, A., Somerscales, R., & Wynn, G. 2004, in IAU Colloq. 190, Magnetic Cataclysmic Variables, ed. S. Vrielmann & M. Cropper (ASP Conf. Ser. 315; San Francisco: ASP), 216
Ramsay, G., Bridge, C. M., Cropper, M., Mason, K. O., Córdova, F. A., & Priedhorsky, W. 2004, MNRAS, 354, 773
Rodríguez-Gil, P., Casares, J., Martínez-Pais, I. G., Hakala, P., & Steeghs, D. 2001, ApJ, 548, L49
Scargle, J. D. 1982, ApJ, 263, 835
Schmidt, G. D., Stockman, H. S., & Smith, P. S. 1992, ApJ, 398, L57
Schmidt, G. D., et al. 2005, ApJ, 630, 1037
Schwope, A. D., Brunner, H., Hambaryan, V., & Schwarz, R. 2002, in ASP Conf. Ser. 261, The Physics of Cataclysmic Variables and Related Objects, ed. B. T. Gänsicke, K. Beuermann, & K. Reinsch (San Francisco: ASP), 102
Schwope, A. D., Schwarz, R., Sirk, M., & Howell, S. B. 2001, A&A, 375, 419
Shafter, A. W. 1983, ApJ, 267, 222
Sirk, M. M., & Howell, S. B. 1998, ApJ, 506, 824

Stellingwerf, R. F. 1978, ApJ, 224, 953
Strüder, L., et al. 2001, A&A, 365, L18
Szkody, P., et al. 2003a, AJ, 126, 1499
———. 2003b, ApJ, 583, 902
Turner, M. J. L., et al. 2001, A&A, 365, L27
Warner, B. 1995, Cataclysmic Variable Stars (Cambridge: Cambridge Univ. Press), 57
Wickramasinghe, D. T., & Ferrario, L. 2000, PASP, 112, 873
Woudt, P. A., Warner, B., & Pretorius, M. L. 2004, MNRAS, 351, 1015
York, D. G., et al. 2000, AJ, 120, 1579